Spatial variability of the erodibility of fine sediments deposited in two alpine gravel-bed rivers: The Isère and Galabre

Hanna Haddad, Magali Jodeau, Cédric Legout, Germain Antoine, Ian Droppo

Spatial variability of the erodibility of fine sediments deposited in two alpine gravel-bed rivers: The Isère and Galabre.

Hanna Haddad[1,2,3], Magali Jodeau[2,3], Cédric Legoût[1], Germain Antoine[2,3] and Ian G. Droppo[4]

[1]Institute for Geosciences and Environmental research (IGE), UGA, CNRS, IRD, INPG, Grenoble, France.

[2]National Laboratory for Hydraulics and Environment (LNHE), EDF R&D, Chatou, France.

[3]Saint-Venant Laboratory for Hydraulics (LHSV), ENPC, Cerema, EDF R&D, Chatou, France.

[4]Environment and Climate Change Canada, 867 Lakeshore Road, Burlington, ON L7R 4A6, Canada

Corresponding Author: Hanna Haddad: hanna.haddad1995@gmail.com

Abstract

In mountainous environments, high suspended sediment load during runoff or dam flushing events can lead to important amounts of fine deposits in gravel bed rivers. Fine sediment deposits may contribute to bar elevation, riparian vegetation growth and consequently to bar stabilization. Despite their contribution to the morphodynamic of mountain rivers, the erosion properties of fine sediments in this context is not fully understood.

In order to investigate the dynamics of re-suspension of these deposits, field monitoring campaigns were performed to explore both the spatial variability and the controlling factors of the erodibility of fine deposits. A cohesive strength-meter (CSM), along with moisture, grain sizes, geographical position and elevation were used to evaluate both the critical bed shear stress for erosion and erosion rate of fine sediment deposits in two rivers of the French Alps: the Isère and Galabre.

The results highlight a large variety of fine sediment deposition areas, which are discontinuous compared to those in estuaries and lowland rivers. A high spatial variability of erodibility was observed on the reach, the bar and the metric scale. While no upstream-downstream trend was observed at the scale of both studied reaches, the locations of the deposits, elevation from the river surface and their moisture were inter-related variables and with the highest correlations to erodibility. Measurements showed that

both dry and humid deposits located at the highest and lowest elevation from the river surface respectively, were more easily eroded than intermediate deposits with medium moisture.

Keywords: Gravel bed rivers, monitoring, fine sediments, erodibility, CSM, sediment properties

1. Introduction

While suspended sediments (SS) are an essential aspect of river dynamics, their delivery from hillslopes to rivers have important environmental issues. They can contribute to the siltation of reservoirs (Syvitski 2005; Kondolf et al. 2014), degradation of aquatic habitats, alteration of fish respiratory organs and export of nutrients or contaminants downstream (Owens et al., 2005; Tritthart et al. 2019). Moreover, high turbidity levels result in significant additional costs for drinking water treatment. Although fine suspended particles have very low settling velocities (particularly under turbulent environments), they encounter various stages of deposition and re-entrainment during their transport from source zones to river outlets (Fryirs 2013; Wilkes et al. 2018).

In mountainous rivers, SS load can be very high due to steep slopes of the headwater streams, the proximity to highly connected sediment source areas as well as the occurrence of heavy rainfall events and intense snowmelt episodes (Zabaleta et al. 2007). Additionally, mountainous rivers have a higher potential to capture and store fine sediments than lowland rivers due to their specific morphology, riverbed large particle size distributions (large void volume) and highly intermittent sediment fluxes (Navratil et al. 2010). Misset et al. (2021) showed that the amounts of fine sediments that are stored in alpine gravel bed rivers can be of equivalent to the mean annual SS yield. In general, two types of in-channel deposits can be distinguished, those stored in the gravel bed matrix and those located at the surface of bars. When the gravel bed itself is mobilized, the fine sediment stored in the voids are entrained as well (Park et al. 2017; Misset et al. 2019). This implies long storage periods of fine particles

in the gravel bed matrix due to the high intermittency of bedload pulses caused, in turn, by the necessity to reach critical flows for bedload activation (Aigner et al. 2017, Rainato et al. 2020). On the other hand, the superficial deposits can be stored and re-entrained without the mobilization of the bed itself, due to the cycles of submergence and dewatering of the bars occurring with each flood event. The frequency of deposition and release of these surface sediments may therefore be greater than for deposits stored in the bed matrix. Although the specific dynamics of superficial deposits has important implications, particularly in relation to mitigating the consequences of dam flushing (Antoine et al. 2020) and to correctly assess SS fluxes downstream of dams, it remains poorly studied and understood mainly due to the large diversity of these surface deposits. In this sense, Wood and Armitage (1999) proposed four categories of fine sediment deposits in function of their locations: marginal deposits, secondary channel deposits, fine superficial laminae deposits, and obstruction and vegetation deposits. Due to their variety of locations, the deposition and erosion of these fine sediment zones is driven by a larger range of discharges than infiltrated deposits and over a larger period of the year.

Both the hydrodynamic aspect, i.e. properties of the flooding events (such as duration of the event, maximum discharge and SS concentration) and the variability of the physical nature of fine particles play essential roles in SS deposition and erosion dynamics. Therefore, physically-based distributed numerical models are tools that can help in understanding and predicting these dynamics. In such models the erosion of fine cohesive sediments is usually represented by the Partheniades erosion law which involves two essential variables describing the erodibility of fine sediment deposited in the river bed: the critical erosion shear stress and the erosion rate of the sediment (Partheniades, 1965). Both variables are controlled by multiple factors. Particle sizes have been historically considered as controlling factors of the erosion for coarse particles ($d > 60$ μm) with the well-known Shields curve (Shields, 1936; Guo, 2020). Due to cohesion, such a relationship does not exist for fine sediments. More recent studies on fine sediments found significant correlations between erodibility and granulometry derived parameters

(Aberle et al., 2006; Grabowski et al., 2011). Other studies found relations with the shear strength of the sediment (Watts et al., 2003; Liu et al., 2018) and others insisted on antecedent moisture of the soil (Singh and Thompson, 2016). Several studies also reported a high spatial variability of fine deposited sediment erodibility, but most of them dealt with estuaries and lowland rivers (Bale et al. 2006; Grabowski et al. 2012; Harris et al. 2016; Joensuu et al. 2018; Liu et al. 2018; Tolhurst et al. 2006; Watts et al. 2003; Widdows et al. 2007). Due to the strong influence of mountain riverbed morphology on the hydro sedimentary regime, it seems essential to investigate also the spatial variability of fine deposit erodibility. Legout et al. (2018) presented a first attempt to assess this variability using a UMCES-Gust Erosion Microcosm System (U-GEMS) (Dickhudt et al., 2011). Their results showed a high degree of spatial variability, however, the limitations of the U-GEMS [i.e., unable to create high enough erosion shear, and the length of time for assessing erodibility (logistics did not allow for cores to be analyzed on site)], were believed to have clouded the extent to which this variability is propagated. They concluded that the 23 cores of their study were not sufficient to capture all the spatial variability, thus highlighting the need to perform the maximum number of measurements on-site within or close to the river bed. The Cohesive Strength-Meter (CSM; MK4, Partrak) (Tolhurst et al. 1999) was employed in this study as it allowed for the rapid measurement of the two variables of interest (critical erosion shear stress and the erosion rate) and perform a large number of measurement in a short duration of time (Tolhurst et al. 2009).

Extensive field monitoring at two mountain rivers was performed to improve our understanding of fine sediment erodibility with the aim to; (i) assess the small-scale (deposit zone) and large scale (bar or reach) spatial variability of the erodibility of fine deposited sediments and (ii) investigate what are the main controlling factors of erodibility in gravel bed rivers. Two main categories of factors were assessed as possible controls of erodibility of fine deposits: (i) those related to the morphology of the river and (ii)

the inherent characteristics of watersheds. Study sites were chosen to be complementary in order to achieve results that are not site specific.

2. Study sites and methods

2.1. Study sites and monitoring areas

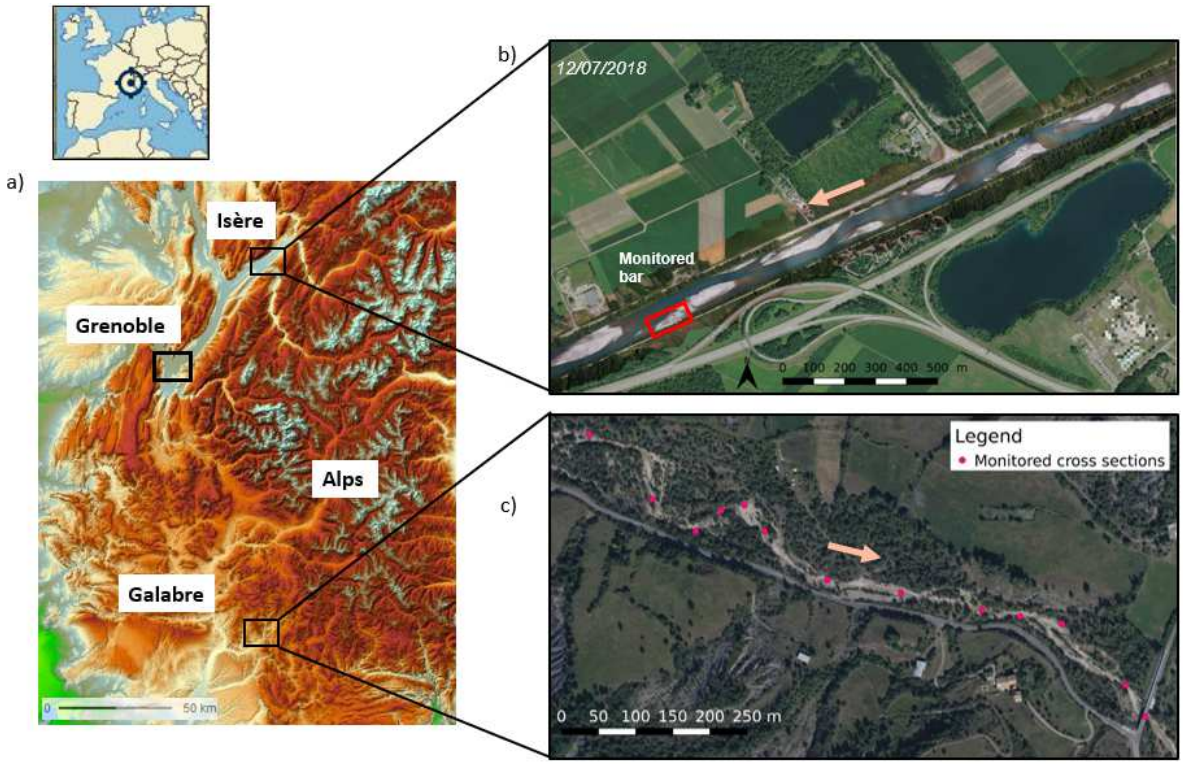

Figure 1 – a) Map of the south east of France with the location of both study sites, (b) zoom on the Isère study site and location of the monitored bar, (c) zoom on the Galabre reach and monitored cross sections.

The morphological features of the river including its width, slope, the position and elevation of gravel bars, and the gravel grain sizes of the bed, may impact the locations and conditions of deposits of fine particles. The inherent characteristics of the upstream watershed including its size, hydro-sedimentary regime, the location, connectivity and pedo-geology of the erosion zones are supposed to impact the nature and grain sizes of the fine particle as well as their deposit dynamics. The two studied sites, the

Isère and Galabre, have been selected as representative of Alpine gravel bed rivers while exhibiting complementary and contrasted morphologic and watershed characteristics.

The Isère River is located in the northern French Alps (Figure 1a,b) and drains a watershed of 2576 km² in the Combe de Savoie reach upstream of the Isère-Arc confluence (Jourdain, 2017). It is part of the ZABR observatory ("Zone Atelier du Bassin du Rhône" [Rhône basin Long Term Environmental Research Observatory]) and has been monitored since 2006 (Thollet et al. 2021). It is embanked, rectilinear and about 100 m wide, with a bed slope of around 0.1 %. It is composed of comparable alternate gravel bars developed in response to channelization and dam construction (Serlet et al., 2018). Grain size measurements performed in 2014 and 2018 on multiple bars in the Combe de Savoie 40 km long reach upstream of the Isère-Arc confluence showed no spatial and temporal differences. Median diameter, 16^{th} and 84^{th} percentiles of gravels composing the bars are respectively 28 mm, 11 mm and 52 mm. The gravel bars are partially covered by vegetation and wood debris contributing to the stabilization of the gravel bars (Jourdain et al., 2019). A significant amount of fine sediments is transported in the river during natural runoff events and the flushing of the Aigueblanche dam, located 40 km upstream of the study site. The annual average SS flux is 1500 10^3 $Mg.yr^{-1}$ in Montmélian corresponding to a specific average SS yield of 310 $Mg.km^{-2}.yr^{-1}$ (Thollet et al. 2021). Mean winter discharges are 150 m^3/s and can reach over 250 m^3/s during flushing events, in spring (Antoine et al. 2020). The average suspended sediment concentration (SSC) is less than 1 g/L most of the time but can reach more than 10 g/L during runoff or flushing events. The large size of the catchment with erosion zones located far from the studied site lead to well mixed SS, i.e. to a homogeneous nature of particles transported (Nemery et al., 2013) and deposited over the bars. Legout et al. (2018) showed that the fine sediment deposits are mostly non-organic and sandy with a non-negligible amount of cohesive sediments (reported median grain sizes around 70 µm, standard deviation of 30 µm and a fine fraction exceeding 40%). In this present work, It is assumed that the studied 400 m long single bar located 1 km upstream the Isère-Arc confluence (Figure

1b) is representative of the bars on the Isère River in Combe de Savoie in terms of morphology and material size.

The Galabre River is located in the southern French Alps (Figure 1a,c) and drains a watershed of 20 km². It is monitored since 2007 (Legout et al. 2021) and the catchment is part of the Draix-Bléone research observatory belonging to the French network of critical zone observatories (OZCAR) (Gaillardet et al. 2018). This river is not regulated by dams. Its width varies between 5 m to 30 m and the mean slope is 2% on the studied reach. Throughout the year, the water discharge in the river is under 1 m^3/s most of the time but can go up to 25 m^3/s during major events in the winter. High amounts of fine sediments are also transported, particularly in summer with SSC up to more than 100 g/L resulting to a mean annual specific SS yield of 670 $Mg.km^{-2}.yr^{-1}$ (Esteves et al. 2019). While the median effective diameters of SS are small (10 µm), they are aggregated at various levels and exhibit either a stability or variability at the event scale (Grangeon et al., 2012). The fine particles fluxes and deposits originate from badlands developed in two lithologies, marls and molasses, which are both or individually activated during rainfall runoff events depending on the spatiotemporal variability of rainfall (Uber et al., 2021). The deposits are thus more heterogeneous in terms of nature compared to those in the Isère. The hydro-sedimentary regime is also more intermittent in the Galabre than the Isère: half of the sediment flux being transported during 2.4% of the time in the Isère near Grenoble whereas it is transported during only 0.13% of the time in the Galabre. The Galabre River contains multiple (dis)-connected channels, creating a greater spatial diversity of deposit compared to the Isère river. The bed material includes gravel (field measurements led to median diameter and 16^{th} and 84^{th} percentiles respectively of 35 mm, 4.3 mm and 93 mm) as well as sandy and cohesive fine sediment deposits. Measurements were done on a 1 km-long reach (Figure 1c) located 2km upstream of the Galabre-Bès confluence.

Four types of surface fine sediment deposits, specific of deposits in mountainous gravel bed rivers are found on both study sites: superficial deposits on gravel bars, secondary channel deposits, marginal

deposits and bar tail deposits (Figure 2). The superficial deposits, positioned higher in elevation, are in contact with water less frequently than the other deposits: the discharge has to be high enough in order to cover them. The deposits in secondary channels, even though they are lower in elevation, are in contact with water only during some events, when secondary channels are connected. Marginal and bar tail deposits are much closer to the water level and are frequently underwater.

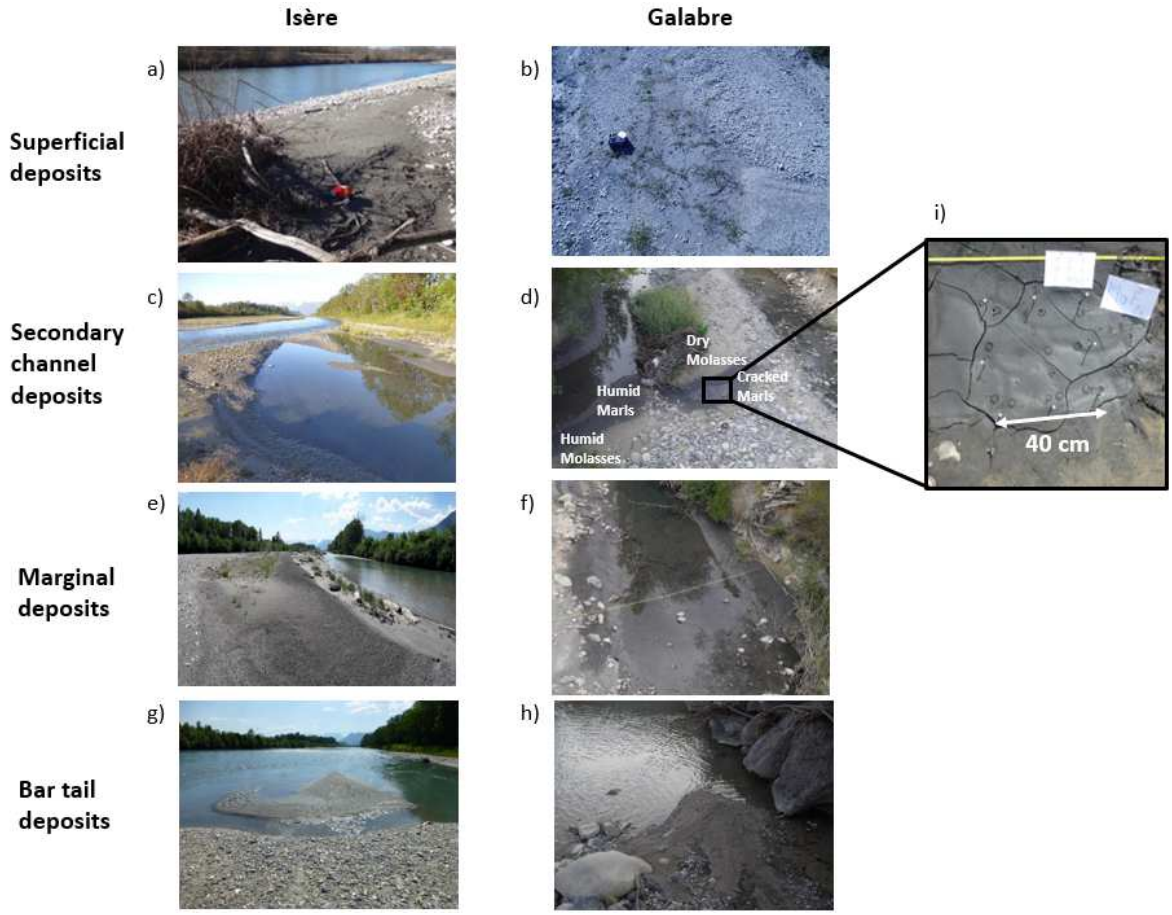

Figure 2 – Examples of fine sediment deposits in superficial areas on the Isère (a) and Galabre (b); in secondary channels in the Isère (c) and Galabre (d); in marginal areas to the flow in the Isère (e) and Galabre (f) and on bar tail areas in the Isère (g) and Galabre (h). (i) Zoom on a measurement area (the Z6 zone) in the Galabre.

2.2. Field sampling and measurements

Two extensive field campaigns were conducted in August 2019 and in July 2020, respectively on the Galabre River and Isère River, in order to assess fine sediment deposit surface, thickness, volumetric moisture and erodibility. During each campaign, 10 to 78 measurement points were defined in the main areas of surface fine sediment deposits. Where possible, these measurement points were placed on a transect perpendicular to the direction of flow. For each measurement point the four pre-cited measurements were performed in a 0.5 m² area. Samples from the top few millimeters were collected and stored in a cold chamber for complementary grain size measurements in the laboratory.

2.2.1. Monitoring strategy on each study site

2.2.1.1. Large scale monitoring

For the Galabre site, the measurements were done on 13 cross sections (transects) perpendicular to the water flow on the 1 km reach (Figure 1c). On each transect, deposit facies were visually delimited by the color, the position (superficial, marginal, under-water) and the physical state of the deposit (smooth, cracked). One measurement point on each facies was selected to represent the deposit.

For the Isère site, measurements were operated where fine deposits were available and for the different types of deposits (i.e. marginal, superficial, behind vegetation or wood debris) on the downstream part (100 m) of the monitored bar (Figure 1b), not necessarily organized by transects as for the Galabre. It was not possible to visually identify different types of deposits since all the fine sediments had the same color on this site. Therefore, the deposits were only characterized by their location, elevation and moisture content.

2.2.1.2. Small scale monitoring

An area on the Galabre River (Z6 zone – Figure 2d), located 620 m from downstream, was used to assess the local small scale variability of sediment properties on the Galabre site. This area comprised the four

188 different facies of deposited sediments that were visually identified along the 1km-long studied reach of
189 the Galabre river (Figure 2d): cracked black deposits coming from badlands in black marl geological zones
190 upstream in the catchment (cracked marl), humid black deposits also issued from marly badlands (humid
191 marl), dry yellowish deposits mainly coming from badlands in molasse geological areas and humid
192 yellowish deposits also issued from molassic badlands (dry and humid molasses). Legout et al (2013)
193 provides details on these different sources of sediments in the Galabre catchment. Erodibility and
194 moisture measurements were done on each facies over a small area of 40cm x 40cm (Figure 2h).
195 On the Isère site, it was not possible to apply the same measurement strategy as the one
196 implemented on the Galabre river to assess the small-scale variability due to: 1) the inability to visually
197 identify different facies on the Isère (i.e. no color difference as on the Galabre), and 2) the reduced
198 number of measurements possible due to i) the limited spatial extent and thickness of the depositional
199 zones in the Isère and ii) the sandy nature of some deposits which did not allow measurements to be
200 made with the CSM (e.g. infiltration problems during measurements). Each erodibility measurement was
201 however replicated 2 to 3 times on the same point, depending on the spatial extension and thickness of
202 the deposits, in order to have an idea of the metric scale variability. Moisture measurements were
203 repeated 10 times in order to have a representative mean value and standard deviation for the deposit
204 area. The measurements were slightly separated (<20 cm) from each other to limit the measurement's
205 impact on the deposit. The locations of deposit zones were characterized by their distance from
206 downstream of the bar.

207 #### 2.2.2. In-situ erodibility measurements

208 Erosion thresholds were identically quantified using the CSM for all sample points on both rivers. The
209 erodibility measurement protocol was the same for all the points and both sites and is the following. The
210 CSM chamber was inserted approximately 1 cm into the sediment deposit and filled with clear water.
211 The CSM test is fully automated, it is based on a vertical water jet impacting the sediment bed and the

increasing pressure induces sediment erosion. This erosion creates turbidity in the CSM chamber which is monitored through infrared light transmission. Starting with a jet pressure of 3.45 kPa and a jet duration of 0.3 sec., every 6 sec. an incremental increase in pressure of 3.45 kPa was applied until 34.45 kPa was achieved. At this point, the pressure increment increased to 6.89 kPa until reaching the max pressure of 413 kPa.

2.2.3. Other in situ measurements: sediment width, thickness and moisture

The thickness, dimensions (length and width) and the volumetric moisture (%) of the fine sediment deposits were measured using a ruler, a decameter and a Delta-T SM150 probe, respectively. This latter integrates moisture over the top 5 cm. These measurements were repeated three to five times at each monitored point and the mean values were used in the following analysis.

2.2.4. Laboratory grain size measurements

Particle size distributions (PSD) were measured with a laser diffraction sizer (Malvern, Mastersizer 2000) following the method of Grangeon et al. (2014) and Wendling et al. (2016). For each sample, three indicators are extracted for the effective (E) and absolute (A) PSD: median particle sizes in µm (Ed_{50} and Ad_{50}), fine percentages (Efine% and Afine% defined as the fraction of particles below 63 µm) and particle ranges in µm (EPR and APR) defined by equation (1). A median disaggregation index (DA in %) was also defined by equation (2).

$$PR = d_{84} - d_{16} \quad (1)$$

$$DA = \frac{\mathrm{Ed50} - \mathrm{Ad50}}{\mathrm{Ad50}} * 100 \quad (2)$$

2.3. Data processing - Extraction of critical jet pressure and suspension index from CSM measurements

For each CSM measurement, an erosion profile (Figure 3) was obtained by plotting the mean optical transmission (%) measured by the CSM at each pressure increment versus jet pressure (kPa). A decrease

in the transmission corresponded to erosion of the sediment. The erosion profile was thus divided in three parts as described by Tolhurst et al (1999): an initial horizontal profile with near 100% transmission, a second part with a drop in transmission and a final horizontal profile where transmission is very low. The three parts of the CSM erosion profile were obtained by fitting the signal with three continuous linear regressions with least squares (Jekel and Venter 2019). The breakpoint that separates the first and the second lines corresponded to the transition between the first and the second part of the signal. It defined the critical jet pressure, expressed in kPa. The suspension index (S_i: %/kPa) defined by Tolhurst et al. (1999) corresponded to the slope of the second part of the CSM signal.

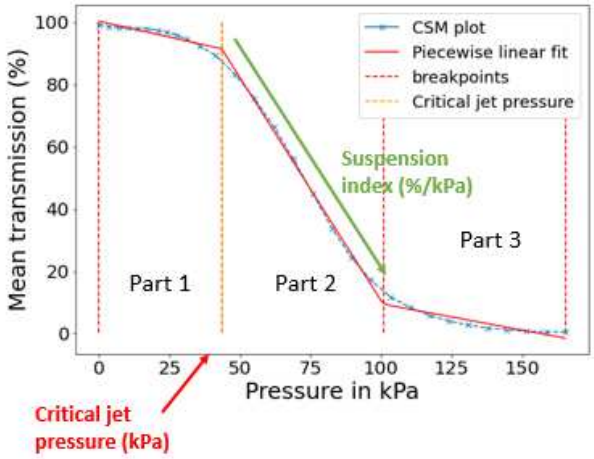

Figure 3 – Examples of a CSM signal separated in 3 parts with piecewise linear fitting and definition of critical jet pressure and suspension index.

3. Results and discussion

3.1. Runoff events prior to monitoring campaigns

Four summer rainfall runoff events took place on the Galabre River prior to the August 2019 monitoring campaign (Figure 4a). Although these events were not associated with high discharge peaks, the SSC reached high values leading to important SS fluxes. The July 1, 15 and 27 events transported principally molasse sediments at high concentrations (up to 200 g/L for the first one) and exhibited medium to

250 relatively high discharges (from 1 to 4.5 m^3/s). The event that occurred August 23 (three days before the
251 monitoring campaign) exhibited lower discharges compared to the others (max discharge 0.1 m^3/s, twice
252 the baseflow) but transported an important amount of marl particles (max SSC 26 g/L). The different
253 characteristics of the above events [discharge, SSC and source sediment (yellow molasse vs. black marl)]
254 and their chronology explain the spatial distribution of the deposits. The marl particles correspond to the
255 superficial deposits within the limits of the flooded area during the last flood (August 23), while the
256 molasse particles are present both under the marl deposits close to the flow and at higher elevations on
257 the banks flooded during the events that occurred in July (see supplementary material).
258 For the Isère River, the discharges vary daily due to snow melting and dam management. It varied
259 between 50 and 150 m^3/s in June 2020 (Figure 4b). The major flood preceding the monitoring campaign
260 took place in the beginning of May (between the 1st and 5th of May) and exhibited discharges over 300
261 m^3/s and SSC up to 3 g/L. Three other smaller events took place during May with discharges higher than
262 200 m^3/s and SSC reaching 1 to 2 g/L. A last event with a maximum discharge of 150 m^3/s and maximum
263 concentration of 1.5 g/L occurred 2 days before the survey in July. During the survey in July, two types of
264 deposits were present, i) newly deposited sediment within the flow path of the last event (July 2, 3) (in
265 marginal areas) given it was deposited during a medium flow event and ii) older consolidated deposits
266 from earlier events in May and July that settled out at higher elevations on the study bar because of
267 deposition at high flows.

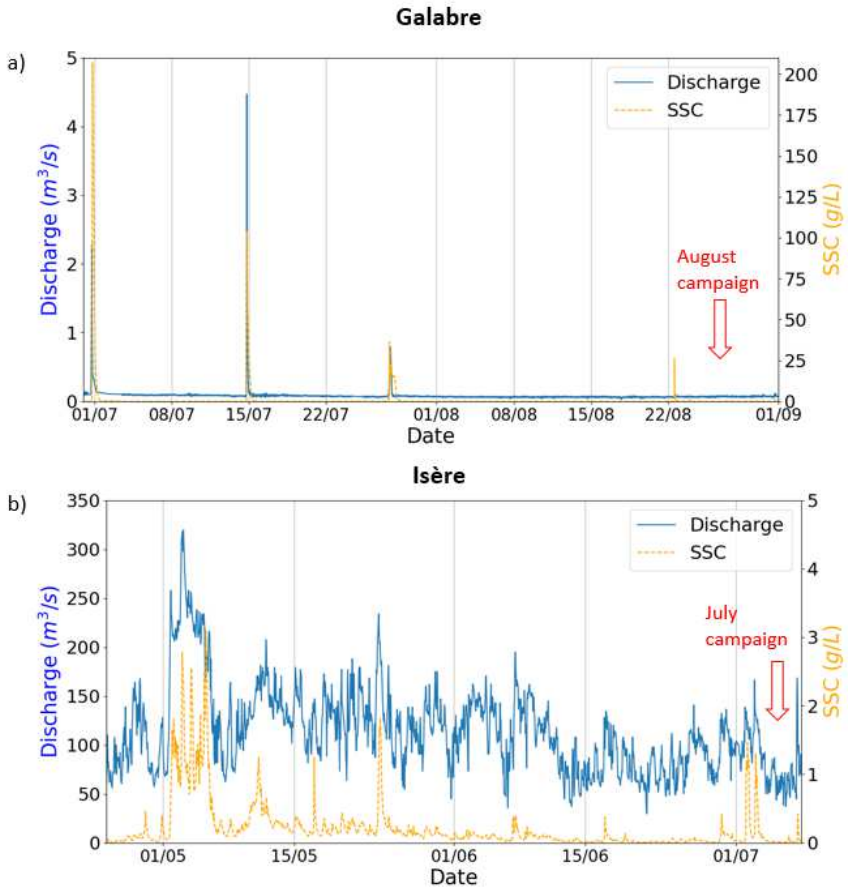

Figure 4 – Discharges and SSC during the two months preceding the monitoring campaigns on (a) the Galabre River and (b) the Isère River. The Galabre data is provided by the monitoring station located 1.5 km upstream of the study site at La Robine sur Galabre. Details on the measurements performed at this station are provided in Legout et al., 2021. The Isère discharge data is provided by the gaging station at Grignon located 15 km upstream of the studied bar and the SSC data by the gaging station at Grésy located 4 km upstream of the studied bar. Details about both stations are given in Bel et al. (2019).

3.2. Grain size measurements and sediment type

The particle size distributions showed that the sediments from the Isère River were coarser than sediments from the Galabre River (Figure 5 and Table 1). For the Galabre site, the black marl deposits were finer than the molasse deposits with effective particle size distribution almost entirely in the cohesive range (Figure 5a) and both the effective and absolute median diameters under 63 µm (Figure 5b). Conversely the molasses exhibited a mean effective median diameter close to 63 µm. However,

their absolute diameters were smaller, in accordance with the important disaggregation index (mean DA = 58.4) (Figure 5b). The effective particle size distributions of the Isère sediments were mostly sandy with a mean effective median diameter of 140.1 µm. The Isère sediments also had the highest particle ranges with an EPR of 213.8 µm and an APR of 177.7 µm (Table 1) showing a large mixture of different particles within a deposit area. The more dispersed distribution and larger sediment sizes for the Isère River compared to the Galabre was mainly explained by the nature and the origin of the fine particles. While the Galabre is narrower and steeper, it does generate a higher transport (and deposition) of larger grain sizes than in the Isère River. However, the Galabre River is highly connected to highly erodible source zones (badlands in marls and molasses) producing important amounts of very fine particles (Grangeon et al., 2012) some of which deposit during the falling limb of runoff events.

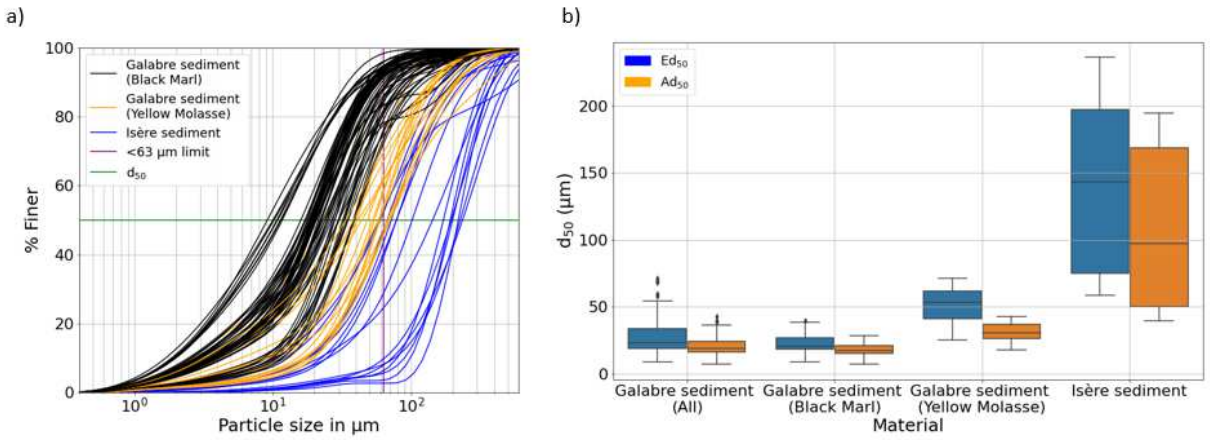

Figure 5 – (a) Effective particle size distribution for the three sediment types: marls (black lines), molasses (yellow lines) and Isère sediments (blue lines) and (b) Effective and absolute d_{50} distributions for each deposit type.

Table 1 – Mean and standard deviation (in brackets) of grain size properties for each category of sediment: marls, molasses and Isère sediments. N is the number of samples, Ed_{50} and Ad_{50} the effective and absolute median diameters, DA the median disaggregation index, Efine% the percentage of particles with effective diameters below 63µm, EPR and APR the particle ranges based on effective and absolute diameters.

	N	Ed_{50} (µm)	Ad_{50} (µm)	DA (%)	Efine%	EPR (µm)	APR (µm)

Black marls	82	21 (8.5)	16.6 (5.6)	25.5 (13.6)	89 (7.2)	45.4 (21.7)	32.4 (8.4)
Yellow molasses	34	50.9 (15.4)	31.6 (7)	58.4 (17)	59.5 (11.9)	122.3 (36.2)	86.3 (32.3)
Isère deposits	15	140.1 (68.4)	108.8 (61)	35.5 (14.6)	24.7 (19.4)	213.8 (77.7)	177.7 (87.2)

297

298 3.3. Spatial organization of deposited sediment erodibility

299 The erodibility measurements exhibited a large range of variability for both rivers (Table 2). At some
300 points the fine sediment deposits were very fragile and erosion occurred during the first steps of eroding
301 pressures of the CSM (low thresholds) with minimal values of 0.1 kPa for the Galabre and 1.61 kPa for
302 the Isère. Other deposits were resistant with very high critical jet pressures, up to over 147 kPa for the
303 Galabre and 249 kPa for the Isère. The critical jet pressure values are higher than the values reported by
304 Grabowski et al. (2012) in lowland rivers (River Frome and Bere Stream) with median critical jet
305 pressures ranging from 8 to 14 kPa depending on the monitoring date in their study sites. The maximum
306 values reported by Grabowski et al. (2012) did not exceed jet pressures of 25 kPa.

307 Erosion rates described by the suspension index were also very variable for both sites with a larger
308 range of values for the Galabre. Once erosion occurred, some deposits with high values of suspension
309 index were eroded rapidly whereas others were eroded slowly. The mean suspension index was higher
310 for the Galabre than for the Isère (Table 2). Thus, once the erosion process began, the fine sediment
311 deposits were eroded more rapidly in the Galabre than in the Isère. The general finding of high spatial
312 variability in the erodibility measurements corroborated the findings of other studies both in different
313 and similar river contexts (Hanson and Simon 2001; C. Legout et al. 2018) and underlined the need to
314 assess some drivers of this heterogeneity.

315 *Table 2 – Statistics on CSM measurements over the Galabre reach in August 2019 and Isère reach in July 2020.*

Galabre 08/2019	**N**	**Mean**	**Standard deviation**	**Min**	**Max**
CSM critical jet pressure (kPa)	122	19.28	22.09	0.1	147.43

CSM suspension index (%/kPa)	122	3.27	2.83	0.17	13.14
Isère 07/2020					
CSM critical jet pressure (kPa)	35	43.57	45.83	1.61	249.94
CSM suspension index (%/kPa)	35	1.94	1.32	0.11	5.9

316

317 ### 3.3.1. Reach and bar scale

318 The longitudinal variability of erosion measurements on both study sites is presented in Figure 6. For the
319 Galabre, most of the critical jet pressure values on the different transects were roughly between 0 and
320 50 kPa. Some values were however higher, for example the maximum point at 70 m from downstream
321 (147.43 kPa) and some measurements at 300 m and 620 from downstream with values higher than 70
322 kPa (Figure 6a). The same conclusions can be derived for the suspension index. All the measurements on
323 the Galabre deposited sediments had the same range of values independently of the transect position.

324 The same was observed for the Isère River measurements in July 2020 (Figure 6b). Thus, there was no
325 upstream/downstream differentiation of the erosion properties of deposited sediment in both rivers.

326

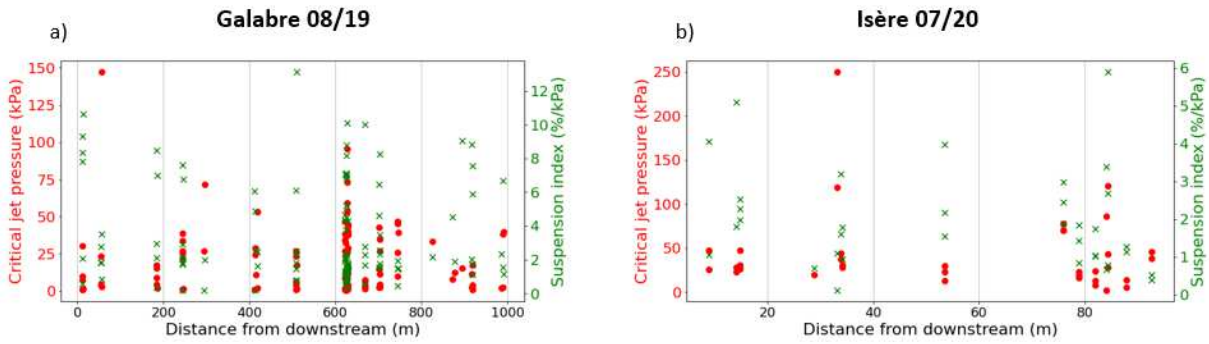

327

328 *Figure 6 – Longitudinal variability of CSM critical jet pressure and suspension index for (a) the Galabre River in August 2019 and*
329 *(b) the Isère River in July 2020.*

3.3.2. Metric scale

Given the lack of observed trends at the river reach scale, we assessed the variability of erodibility at the metric scale. The 49 CSM measurements performed in the Z6 zone of the Galabre River (620 m from downstream) on the different facies of deposits (cracked marl, humid marl, humid molasses, dry molasses) were used to assess the small-scale local variability of sediment properties. Nine measurements were done on each area of 40 cm x 40 cm (0.16 m²) (Figure 2i) except for the humid molasse deposits where 11 measurements were done on the facies.

Table 3 – Mean and standard deviation (in brackets) of sediment properties for the four different visually identified facies of deposits in the Z6 area on the Galabre River in August 2019.

Sediment facies	Critical jet pressure (kPa)	Suspension index (%/kPa)	Ed_{50} (µm)	Moisture (%)
Cracked marl	43.3 (31)	1.1 (0.4)	10.2	46.2 (3.3)
Humid marl	22.2 (17.3)	2.1 (1.4)	17.8	48 (7.1)
Humid molasse	30.5 (16.1)	1.8 (0.9)	38.5	31.7 (5.8)
Dry molasse	2.5 (3.5)	6.1 (2.1)	68	9.5 (1.9)

The raw CSM signals displayed a large variability of the measurements between the four facies of deposits (Table 3 and Figure 7a). Indeed, signals corresponding to the dry molasse exhibited a very high slope at the beginning of the CSM test and reached rapidly a transmission of 0% between 30 and 60 kPa. In contrast, the signals corresponding to the cracked marl facies required higher pressures to begin the erosion process and the second part of the CSM test ended at high pressures, up to 200 kPa. This was confirmed by the calculations of the critical jet pressure and suspension index distributions for each facies (Figure 7b). Non-parametric significance tests were conducted to examine the spatial differences in erodibility (Kruskal-Wallis tests with Bonferroni correction). The dry molasses corresponding distributions were significantly different from the other three facies. The dry molasse was the facies with

349 the lowest critical jet pressure values and the highest suspension index values. It was also the driest
350 facies with the largest grain size (Table 3). In contrast cracked marls were the most resistant with the
351 highest mean critical pressure (43.3 kPa) and the lowest suspension index (1.1 %/kPa). It was the facies
352 with the smallest effective median diameter (10.2 µm). It also exhibited the highest variability of the
353 erodibility (standard deviation of 31 kPa). Even though the cracked marl facies were significantly
354 different from the dry molasse, the distributions of critical jet pressure and suspension index of cracked
355 marls were not significantly different from the humid marl and humid molasse facies. Nonetheless, the
356 humid marl (mean critical pressure of 22.2 kPa) was slightly easier to erode and exhibited lower grain
357 size (Table 3) than the humid molasse (mean critical pressure of 30.5 kPa). Concerning the critical jet
358 pressures, it is important to note that the intra facies variability was high, highlighting an important
359 small-scale variability inside each facies. The suspension index boxes (Figure 7b) were narrower, relating
360 to a lower variability of the erosion rate on this scale, with for example a standard deviation of 0.9 %/kPa
361 for the humid molasse.

362 Even though less measurements were done at the small scale in the Isère compared to the Galabre,
363 some locations displayed a very small variability of the CSM signals. For the measurements located at 13,
364 76, 79, 90 and 95 m from downstream in Figure 6b (2, 2, 3, 2 and 2 measurements respectively), the
365 differences between the measurements on each point were less than 10 kPa and 1 %/kPa, for the critical
366 jet pressure and the suspension index respectively. For these deposit areas, the small-scale erosion
367 variability on the facies was low. However, the measurements were more variable in other deposit areas
368 as shown at 32, 53 and 85 m from downstream in Figure 6b (2, 3, 2 measurements respectively) where
369 the difference can reach 100 kPa for the CSM critical jet pressure and 4 %/kPa for the suspension index
370 in an area of less than 0.5 m^2.

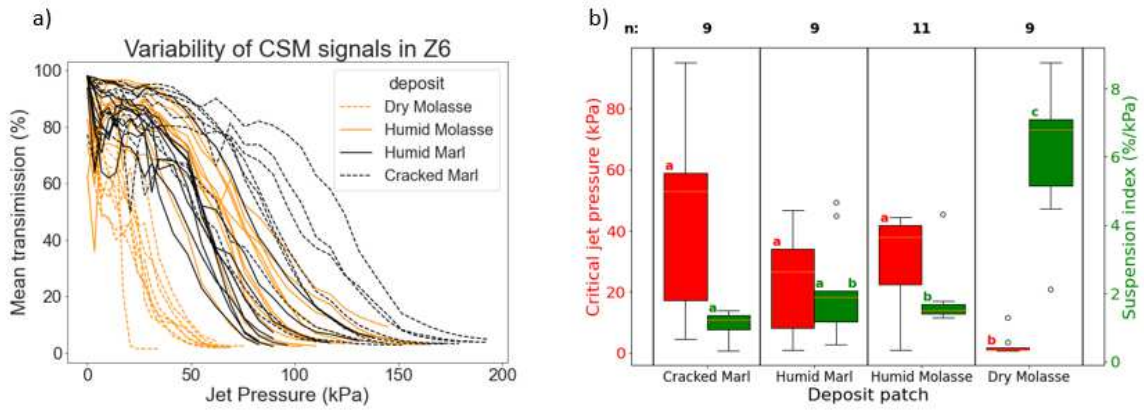

371

372 *Figure 7 – (a) CSM signals grouped by deposit facies identified visually and (b) extracted variables from the signals: critical jet*
373 *pressure and suspension index for the deposited sediment in the Z6 zone in the Galabre River (located 620 m from downstream).*
374 *Facies marked with the same letter have properties that are not significantly different for the considered variable (Kruskal-Wallis*
375 *test with Bonferroni correction, P<0.05).*

376 It should be stressed that the variability observed at the metric scale within facies considered visually
377 homogeneous, are due to both the repeatability of the measurement inherent to the protocol (e.g.
378 mainly related to the insertion of the CSM measuring cylinder in the sediment) and the variability of the
379 deposits themselves. This small-scale variability was also observed by Tolhurst et al. (2006) reporting a
380 high variability between measurements within 1-2 m from each other, partly explained by biofilm areas
381 in their case study. It was also observed by Legout et al. (2018) using the U-GEMS in similar gravel bed
382 rivers.

383 ### 3.3.3. Transect scale

384 As the metric-scale analysis revealed different erodibility patterns between visually identified
385 depositional facies, we evaluated how these measures were spatially organized at the scale of transects
386 perpendicular to the flow. The lateral variability of the sediment properties are illustrated through four
387 transects in the Galabre River (Figure 8) and through one transect on the Isère River (Figure 9). For the
388 Galabre River, superficial deposits (mainly composed of dry molasses) and under-water marly deposits
389 were rapidly eroded by the CSM (low critical jet pressure and high suspension index), whereas marginal

deposits in-between corresponded to the highest values of critical jet pressures and lowest suspension indexes. A comparable lateral organization of the deposits was observed in the Isère River (Figure 9) even though less measurements could be done due to the location and the nature of the deposits. The measurement of the deposited sediment on the top of the gravel bar (approx. 11 m from left bank) had the lowest critical jet pressure and was the easiest to erode. The marginal deposit (23 m from left bank) had the highest critical jet pressure. The closest measurement to the water (27 m from left bank) had a critical jet pressure lower than the previous one and was easier to erode. However, the relation between the suspension index and the position of the deposits was less visible for the Isère River than for the Galabre River.

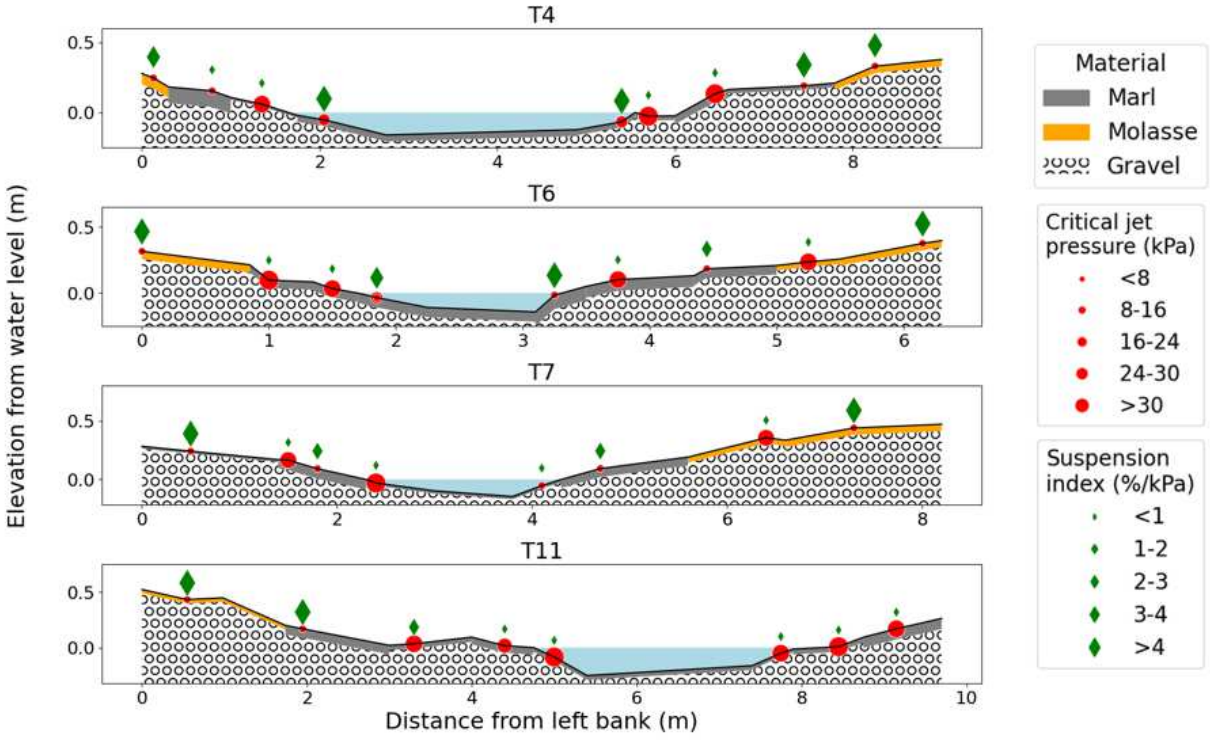

Figure 8 – Four transects on the Galabre River in August 2019 showing different properties of the deposited sediments: surface, material type, thickness, elevation from water level and CSM critical jet pressures and suspension indexes.

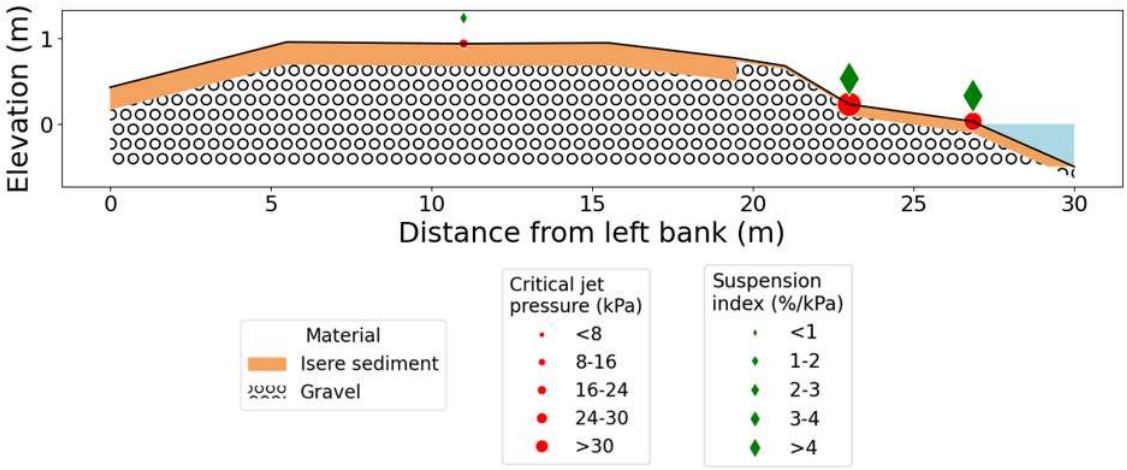

402

403 *Figure 9 – Transect on the Isère River in July 2020 with three CSM measurements showing different properties of the deposited*
404 *sediments: surface, thickness, elevation from water level and CSM critical jet pressures and suspension indexes*

405 Given that the location of the deposit according to the distance or elevation from the water surface
406 seems to be linked to the erodibility of the sediments and that the moisture of the sediments was
407 significantly correlated to their elevation (Table 4), the relationships between CSM measurements and
408 the moisture of sediments were analyzed. For both study sites, measurements were grouped in four
409 categories depending on the moisture from very dry to very humid (Figure 10). The critical jet pressure
410 measured in the Galabre exhibited maximum values for intermediate moisture comprised between 15
411 and 50% (Figure 10a). The suspension indexes exhibited an opposite trend with the smallest erosion
412 rates in the intermediate moisture groups. These deposits tend to be positioned at a medium elevation
413 on the transect scale (Figure 8). On the other hand, for very dry and very humid deposits, corresponding
414 respectively to superficial deposit with a high elevation and under-water deposits with low elevations on
415 the transect, critical jet pressures were low and suspension index values were high, suggesting that these
416 deposits were more easily erodible.

417 On the Isère site in July 2020, most of the CSM measurements were performed on very humid
418 deposits (20 out of 35 measurements in Figure 10b). The critical jet pressures exhibited a similar relation
419 with moisture as the one observed for the Galabre site. Most resistant deposits were those with medium

moistures. Although statistical tests did not identify any significant differences of critical jet pressures between the different moisture groups, there is a tendency of higher pressures for medium humidity. The absence of any significant difference might be related to the smaller number of measurements in low moisture groups due to the lack of dry deposits during the field campaign on the Isère River. This could also explain why high median suspension index values were measured for humid deposits for the Isère (Figure 10b) while more resistant deposits and thus lower values of the suspension index would have been expected according to the general trend on both sites. Beyond these small discrepancies between both rivers, it should be stressed that for each moisture state, the Isère deposits exhibited higher critical jet pressures than the Galabre suggesting more resistant deposits. In the same way, the suspension indexes were lower, except for some of the humid deposits.

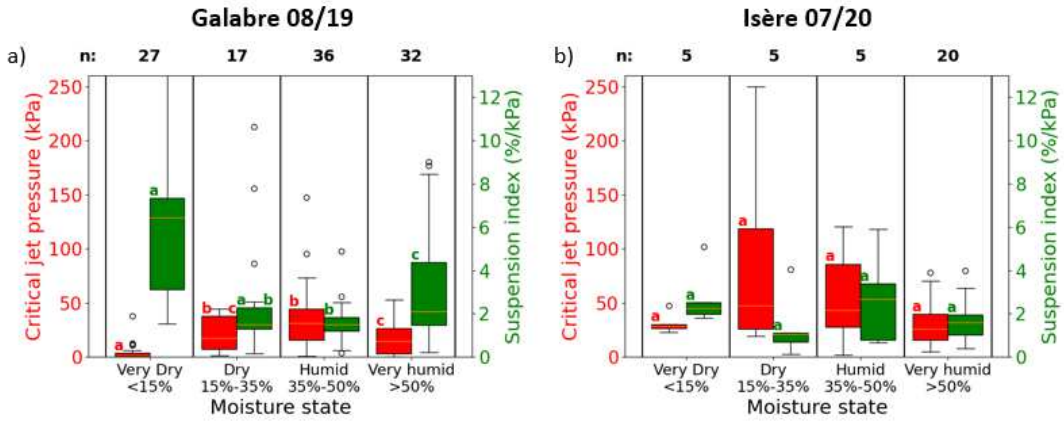

Figure 10 – CSM critical jet pressure and suspension index in (a) the Galabre River in August 2019 and (b) in the Isère River in July 2020 for four groups of moisture: Very dry : <15 % volumetric moisture, dry: 15%-35%, humid: 35%-50% and very humid : >50%. Boxes marked with the same letter have properties that are not significantly different for the considered variable (Kruskal-Wallis test with Bonferroni correction, P<0.05).

3.4. Relationship between erosion measurements and sediment properties

The trends observed between erodibility and moisture at the transect scale led to a more detailed analysis of the relationships between erodibility and the physical characteristics of the deposits. Spearman's rank correlations were used to investigate relationships between erosion measurements and

co-variables relating to sediment properties. The CSM critical jet pressure and suspension index were significantly correlated to all grain size variables but the correlations remained small for the Galabre with maximum values of |R|=0.29 and |R|=0.34 for the critical jet pressure and suspension index respectively (Table 4).

While fewer correlations were significant between erodibility variables and grain size variables for the Isère, the highest correlations were observed for this site between the critical jet pressure and the amount of fine particles (effective and absolute). This suggests that an increasing cohesive part in the sandy deposits of the Isère make them more resistant to erosion. Apart from this correlation, the critical jet pressure was also poorly correlated to effective and absolute median diameters with negative coefficients as for the Galabre site (Table 4). The suspension index was even less correlated to particle sizes in the Isère than in the Galabre. This general observation of very weak correlations between granulometric variables and variables describing erodibility was consistent with that of Legout et al. (2018) on fine sediment deposits also coming from the Isère River further downstream. Whereas granulometric variables are often found to be important controlling factors of erodibility in other environments (Lick and McNeil, 2001; Grabowski et al., 2011), this was not the case in gravel bed rivers. However, similar to our study, observations by Joensuu et al. (2018) showed a negative correlation between erosion threshold and median particle sizes (effective and absolute diameters). The increase of sediment resistance with an increase of the cohesive percentage (or fine fraction - <63 µm) was also reported by Harris et al. (2016); Lanuru et al. (2007); Le Hir et al. (2008); van Rijn (2020).

*Table 4 – Spearman's rank correlation coefficients for the Galabre August 2019 data (inferior diagonal, red data) and for the Isère July 2020 data (superior diagonal, blue data), for CSM critical jet pressure (CSM τ_c), suspension index (s_i), volumetric moisture (% Vol Moist), deposit elevation (Elev), thickness (Thick) and granulometric extracted indices (Ed_{50}, Ad_{50}, Efine%/, EPR, Afine%, APR and DA). Elevation was not available for the Isère data. Numbers marked with * correspond to a 0.01 level of significance of the correlation.*

	CSM τ_c	s_i	% Vol Moist	Elev	Thick	Ed_{50}	Ad_{50}	Efine%	EPR	Afine%	APR	DA
CSM τ_c	-	-0.02	-0.39	-	-0.53*	-0.27	-0.37	0.55*	0.09	0.53*	-0.15	0.31
s_i	-0.56*	-	-0.2	-	-0.22	0.13	0.09	-0.01	0.06	-0.01	0.24	0.15
% Vol Moist	0.29*	-0.29*	-	-	0.48*	0.56*	0.61*	-0.65*	0.42*	-0.68*	-0.52*	-0.69*
Elev	-0.19*	0.24*	-0.77*	-	-	-	-	-	-	-	-	-
Thick	0.07	-0.13	0.1	0.11	-	0.26	0.36	-0.63*	0.05	-0.62*	0.17	-0.64*
Ed_{50}	-0.29*	0.33*	-0.74*	0.83*	0.02	-	0.97*	0.86*	0.64*	-0.86*	0.94*	-0.68*
Ad_{50}	-0.29*	0.34*	-0.72*	0.81*	0.03	0.98*	-	-0.92*	0.59*	-0.93*	0.88*	-0.75*
Efine%	0.2*	-0.21*	0.77*	-0.8*	-0.17	-0.91*	-0.86*	-	-0.42*	0.99*	-0.73*	0.83*
EPR	-0.2*	0.21*	-0.7*	0.81*	0.04	0.94*	0.88*	-0.93*	-	-0.42*	0.73*	-0.28
Afine%	0.13	-0.12*	0.76*	-0.82*	-0.2	-0.86*	-0.85*	0.91*	-0.83*	-	-0.73*	0.85*
APR	-0.21*	0.29*	-0.7*	0.86*	0.07	0.96*	0.96*	-0.88*	0.93*	-0.9*	-	-0.52*
DA	-0.24*	0.23*	-0.71*	0.64*	0.11	0.72*	0.61*	-0.83*	0.75*	-0.76*	0.65*	-

With respect to the observed trend between moisture and erodibility in Figure 10, both the Galabre and Isère exhibited small correlation coefficients either between critical jet pressure and moisture or between suspension index and moisture (|R|<0.4; Table 4). However, the relations between both CSM variables and the moisture were not linear (Figure 10), showing rather an increase followed by a decrease of erodibility while the moisture increased. The correlation analysis was therefore done by separating the data set into two moisture classes: dry sediments with moisture lower than 35% and humid sediments with moisture higher than 35%. The calculated correlations were higher by separating the data in two moisture groups for both sites, even though they were not always significant at a 0.01 level because of a lack of measurements (Table 5). For both sites, the correlation coefficients between the CSM critical jet pressure and moisture, were positive for the dry sediments and negative for the

humid sediments respectively. Opposite trends were observed for the suspension index, except for the Isère humid data.

For both rivers, the CSM measurements exhibited a breakpoint of moisture around 35% separating the erosional behavior of the sediments. With increasing moisture until the breakpoint, the sediment's resistance increased with an increasing critical jet pressure and a decreasing suspension index (Figure 10). When the breakpoint was reached and moisture increased above it, the sediment's erodibility decreased with a decreasing critical jet pressure and an increasing suspension index. This was also observed by Singh and Thompson (2016) and Truman et al. (1990) on their study sites, even though they worked with hillslope soils. They highlighted an important control of the volumetric moisture on the erodibility, explained by different mechanisms involved in the aggregate breakdown occurring during rainfall events (less aggregate breakdown for pre-wetted soils than for soils near saturation). In their study, they reported values of moisture below 40 % and found a breakpoint at 30 %. To the authors' knowledge, it was the only study that found this striking relation between erodibility and moisture. Other studies reported values of moisture but did not have a clear correlation with erodibility. This is likely related to lower ranges of moisture [30 % to 45 % for Lanuru et al. (2007), 26 % to 33 % for Liu et al. (2018)], compared to our range of very dry (less than 10 % volumetric moisture) to very humid (more than 70%).

*Table 5 – Spearman's rank correlation coefficients for the Galabre (inferior diagonals, red data) and the Isère (superior diagonals, blue data) separated in two categories: dry data (Moisture < 35%) and humid data (Moisture > 35%), for CSM jet pressure (CSM τ_c), suspension index (s_i) and volumetric moisture (% Vol Moist). Numbers marked with * correspond to a 0.01 level of significance of the correlation.*

Dry data	**CSM τ_c**	**s_i**	**% Vol Moist**	**Humid data**	**CSM τ_c**	**s_i**	**% Vol Moist**
CSM τ_c	-	-0.19	0.51		-	0.04	-0.54
s_i	-0.76*	-	-0.58		-0.28	-	-0.17
% Vol	0.6*	-0.54*	-		-0.36	0.32	-

Moist

3.5. Specific features of the erodibility in gravel bed rivers

Comparing the erodibility measurements with those from other studies required the conversion of CSM critical jet pressures to critical shear stresses in Pa (N/m^2). Therefore, the CSM vertical jet pressures were converted to equivalent horizontal shear stress using the equation of Tolhurst et al (1999). As this calibration of the CSM was done for sand particles >150 µm using different setting modes than the one used in this study, the equation might not be fully adapted to our range of sediments and jet pressures. This comparison was done only for critical shear stresses and not erosion rates as; (i) most of the CSM studies reported only critical shear stresses and (ii) the erosion rates extracted from CSM measurements cannot be easily compared to other devices since the test time and the applied shear stresses on the deposits are not the same. Bearing in mind these potential limitations, as well as others related to the comparison of different measuring devices with different spatial footprints, some specific features can be noted.

A first noticeable feature is that the studies using larger footprint devices, like GUST chambers (Legout et al., 2018), EROMES (Harris et al. 2016; Joensuu et al. 2018; Lanuru et al. 2007; Widdows et al. 2007) or larger in situ flumes (Meng et al., 2012; Noack et al., 2015) led to lower erosion thresholds than in our study and in all others using the CSM device. This was already reported in studies that compared various devices (Tolhurst et al., 2000; Tolhurst et al., 2009; Widdows et al., 2007). According to Widdows et al. (2007), the differences are related to fundamental differences of the applied stress, the CSM applies a vertical stress on the sediment which is different than devices generating horizontal smooth hydraulic flow such as in situ flumes or annular flumes.

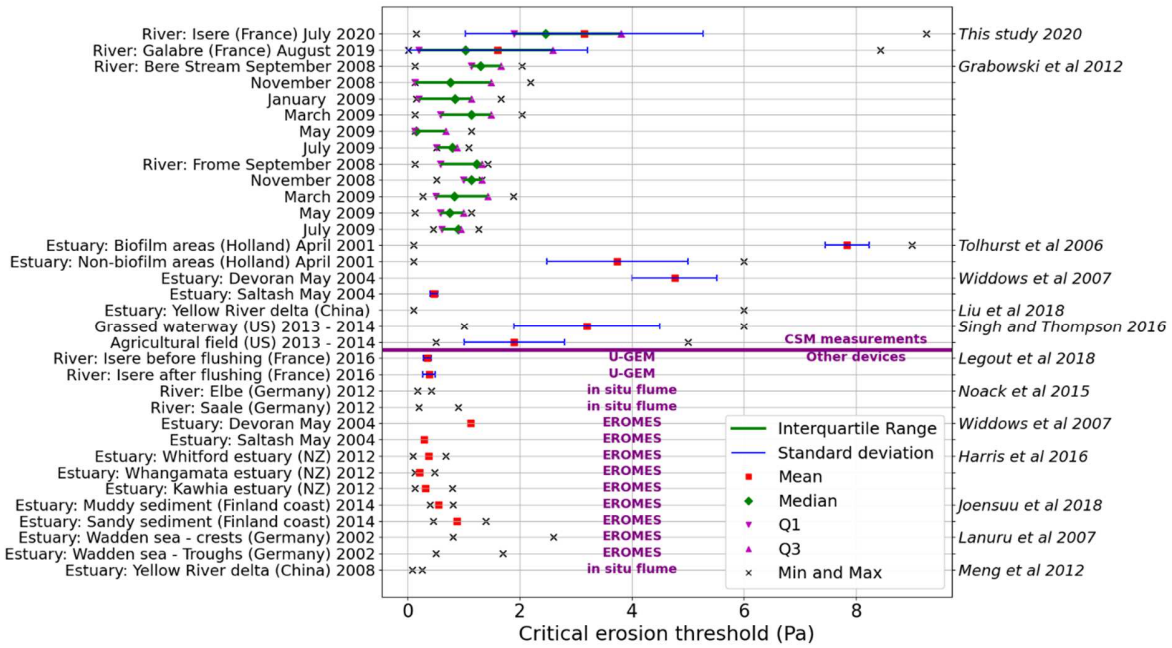

Figure 11 – Critical erosion threshold for this study and other studies for different rivers and estuaries. Statistical variables are plotted depending on the available data in the papers: mean, standard deviation, median, 1st and 3rd quartiles (Q1 and Q3), min and max and interquartile range. Studies using the CSM device are separated from the others. In order to compare in the same units as the other studies, the data acquired from Grabowski et al (2012) was transformed using the calibration of Tolhurst et al. (1999).

A second striking feature is that the mean critical shear stress and its standard deviation derived from this study were well within the reported literature data using the CSM device (Figure 11). Nevertheless, the variability of the erodibility in both studied rivers was one of the highest along with the variability observed by Tolhurst et al. (2006) and Liu et al. (2018) in estuaries and by Singh and Thompson (2016) in agricultural watersheds. In estuaries, the high variability is often explained by areas covered by biofilms (Tolhurst et al. 2006). As no biofilms were observed during the reported field campaigns in the Galabre and Isère, this suggests that the reasons for this large spatial variability are related to both i) the inherent characteristics of the watershed as a provider of fine sediments and a regulator of the hydrosedimentary regime (i.e. discharge and SSC) and ii) the morphological characteristics of the river bed impacting the hydrodynamics and thus the conditions of settling.

The spatial variability of fine deposit erodibility within the catchment can be related to the higher temporal variability of the type (nature, size and SSC) of fine sediments in small mountain rivers than in estuaries. Indeed, fine sediments can originate from different parts of the catchments, as underlined for the Galabre site, thus leading to spatial variations of the sediment physical properties in the river bed according to the successive flood history and their respective magnitude (Figure 4) (e.g. elevation of deposits on gravel bars). This temporal effect controlling the spatial heterogeneity of deposits is assumed to be scale dependent, i.e. marked in small headwater catchments such as the Galabre, less pronounced in river reaches draining medium size watersheds like the Isère and fully smoothed in estuaries draining large upstream areas.

The larger variability measured in this study, compared to other estuarine and riverine environments (Grabowski et al. 2012; Widdows et al. 2007)also underlines the specificity of the morphology of gravel bed rivers compared to lowland rivers. In addition to the fact that gravel bed rivers can store important amounts of fine sediments (Navratil et al. 2010; Misset et al. 2021), their fine sediments exhibit distinct properties, from very erodible to highly resistant. This could be related to the high heterogeneity of the settling conditions controlled mainly by two specific characteristics of gravel bed rivers, operating at two scales. At the reach and transect scale, the topography within gravel bed rivers can be very heterogeneous leading to deposits at different elevations according to the bar morphology and the magnitude of the preceding runoff events. The granulometry of the particles composing the matrix of gravel bed rivers are also very heterogeneous, ranging from sand to boulder. The conditions of deposit of fine sediment are thus discontinuous in space (Camenen et al., 2013) and different from homogenous deposits over mudflats.

4. Conclusions

This paper describes and analyzes erodibility measurements of fine sediments deposited in two Alpine rivers: The Isère and Galabre. Significant spatial variations in the erodibility of fine sediment deposits

were identified. There was no spatial structuration of the erodibility at the reach scale, but a trend was observed at the transect scale. A high variability was observed at the facies scale, related to the local heterogeneity of the deposit but was lower than the variability between different facies. At the transect scale, CSM measurements showed that deposits on medium elevation areas and with medium moisture were more resistant than drier superficial deposits and more humid under-water deposits.

The field campaigns reported in this study showed the need to expand the measurements in order to assess correctly the variability. It highlighted also the importance of the choice of devices and measurement protocols to capture the variability at the relevant scale. Rapid and small-footprint devices, such as the CSM used in this study, are ideal for robust assessments of small and large scale variability over the river.

The variability of erodibility of fine deposits in gravel bed rivers is more pronounced than in other lowland rivers or estuaries. This variability is related to the specificities of gravel bed rivers with deposit conditions discontinuous in space. It is driven by the abundance of areas of deposition with highly variable elevation, moisture and grain size properties, compared to literature results in other environments. Particularly, antecedent moisture appeared as the main controlling factor of the erosion properties.

This study provides insight into the variability of fine sediment properties in gravel bed rivers and will aid in improving numerical models to fully understand and manage fine sediment dynamics in such high energy rivers.

Acknowledgments

This work was funded by the French National Association of Research and Technology (ANRT) and EDF R&D with the Industrial Conventions for Training through Research (CIFRE grant agreement 2018/1453). The authors would like to thank the French national agency (ANR) under the grant ANR-18-CE01-0020 (DEAR project). This study was carried out in Draix-Bleone Observatory funded by INRAE, INSU and OSUG

578 and is part of OZCAR Research Infrastructure that is supported by the French Ministry of Research,
579 French Research Institutions and Universities. We also thank the people who contributed in the field
580 measurements: Théo Woelffel (student) and the EMMN team of the LNHE.

581 References

582 Aberle, J., Nikora, V., Walters, R., 2006. Data Interpretation for In Situ Measurements of Cohesive Sediment Erosion. J. Hydraul.
583 Eng. 132, 581–588. https://doi.org/10.1061/(ASCE)0733-9429(2006)132:6(581)

584 Aigner, J., Kreisler, A., Rindler, R., Hauer, C., & Habersack, H., 2017. Bedload pulses in a hydropower affected alpine gravel bed
585 river. Geomorphology, 291, 116-127. https://doi.org/10.1016/j.geomorph.2016.05.015

586 Antoine, G., Camenen, B., Jodeau, M., Némery, J., Esteves, M., 2020. Downstream erosion and deposition dynamics of fine
587 suspended sediments due to dam flushing. Journal of Hydrology 585, 124763. https://doi.org/10.1016/j.jhydrol.2020.124763

588 Bale, A.J., Widdows, J., Harris, C.B., Stephens, J.A., 2006. Measurements of the critical erosion threshold of surface sediments
589 along the Tamar Estuary using a mini-annular flume. Continental Shelf Research 26, 1206–1216.
590 https://doi.org/10.1016/j.csr.2006.04.003

591 Bel, C., Jodeau, M., Tassi, P., Claude, N. Haddad, H., 2019. Calibration and validation strategy for 2D hydrodynamic modelling:
592 application to morphodynamics of a gravel bed river with suspended sediments. XXVIth TELEMAC-MASCARET User Conference,
593 15th to 17th October 2019, Toulouse. https://doi.org/10.5281/zenodo.3611515

594 Camenen, B., Jodeau, M., & Jaballah, M., 2013. Estimate of fine sediment deposit dynamics over a gravel bar using photography
595 analysis. *International Journal of Sediment Research*, *28*(2), 220-233. https://doi.org/10.1016/S1001-6279(13)60033-5

596 Dickhudt, P.J., Friedrichs, C.T., Sanford, L.P., 2011. Mud matrix solids fraction and bed erodibility in the York River estuary, USA,
597 and other muddy environments. Continental Shelf Research 31, S3–S13. https://doi.org/10.1016/j.csr.2010.02.008

598 Fryirs, K., 2013. (Dis)Connectivity in catchment sediment cascades: a fresh look at the sediment delivery problem:
599 (DIS)CONNECTIVITY IN CATCHMENT SEDIMENT CASCADES. Earth Surface Processes and Landforms 38, 30–46.
600 https://doi.org/10.1002/esp.3242

601 Gaillardet, J., Braud, I., Hankard, F., Anquetin, S., Bour, O., Dorfliger, N., et al. 2018. OZCAR: The French Network of Critical Zone
602 Observatories. Vadose Zone Journal 17, 180067. https://doi.org/10.2136/vzj2018.04.0067

603 Grabowski, R.C., Droppo, I.G., Wharton, G., 2011. Erodibility of cohesive sediment: The importance of sediment properties.
604 Earth-Science Reviews 105, 101–120. https://doi.org/10.1016/j.earscirev.2011.01.008

605 Grabowski, R.C., Wharton, G., Davies, G.R., Droppo, I.G., 2012. Spatial and temporal variations in the erosion threshold of fine
606 riverbed sediments. J Soils Sediments 12, 1174–1188. https://doi.org/10.1007/s11368-012-0534-9

607 Grangeon, T., Legout, C., Esteves, M., Gratiot, N., & Navratil, O. 2012. Variability of the particle size of suspended sediment
608 during highly concentrated flood events in a small mountainous catchment. Journal of Soils and Sediments, 12, 1549–1558.
609 https://doi.org/10.1007/s11368-012-0562-5

610 Guo, J., 2020. Empirical model for Shields diagram and its applications. *Journal of Hydraulic Engineering*, *146*(6), 04020038.
611 https://doi.org/10.1061/(ASCE)HY.1943-7900.0001739

612 Hanson, G.J., Simon, A., 2001. Erodibility of cohesive streambeds in the loess area of the midwestern USA. Hydrol. Process. 15,
613 23–38. https://doi.org/10.1002/hyp.149

614 Harris, R.J., Pilditch, C.A., Greenfield, B.L., Moon, V., Kröncke, I., 2016. The Influence of Benthic Macrofauna on the Erodibility of
615 Intertidal Sediments with Varying mud Content in Three New Zealand Estuaries. Estuaries and Coasts 39, 815–828.
616 https://doi.org/10.1007/s12237-015-0036-2

617 Jekel, C.F., Venter, G., 2019. pwlf: A Python Library for Fitting 1D Continuous Piecewise Linear Functions URL : https://github.
618 com/cjekel/piecewise_linear_fit_py

619 Joensuu, M., Pilditch, C.A., Harris, R., Hietanen, S., Pettersson, H., Norkko, A., 2018. Sediment properties, biota, and local habitat
620 structure explain variation in the erodibility of coastal sediments: Variation in the erodibility of coastal sediments. Limnology
621 and Oceanography 63, 173–186. https://doi.org/10.1002/lno.10622

622 Jourdain, C. Action des crues sur la dynamique sédimentaire et végétale dans un lit de rivière à galets : l'Isère en Combe de
623 Savoie. Hydrologie. Université Grenoble Alpes, 2017. Français. NNT :2017GREAU002.

624 Jourdain, C., Claude, N., Tassi, P., Cordier, F., Antoine, G., 2019. Morphodynamics of alternate bars in the presence of riparian
625 vegetation. Earth Surface Processes and Landforms. https://doi.org/doi: 10.1002/esp.4776

626 Kondolf, G.M., Gao, Y., Annandale, G.W., Morris, G.L., Jiang, E., Zhang, J., Cao, Y., Carling, P., Fu, K., Guo, Q., Hotchkiss, R.,
627 Peteuil, C., Sumi, T., Wang, H., Wang, Z., Wei, Z., Wu, B., Wu, C., Yang, C.T., 2014. Sustainable sediment management in

628 reservoirs and regulated rivers: Experiences from five continents. Earth's Future 2, 256–280.
629 https://doi.org/10.1002/2013EF000184

630 Lanuru, M., Riethmüller, R., van Bernem, C., Heymann, K., 2007. The effect of bedforms (crest and trough systems) on sediment
631 erodibility on a back-barrier tidal flat of the East Frisian Wadden Sea, Germany. Estuarine, Coastal and Shelf Science 72, 603–
632 614. https://doi.org/10.1016/j.ecss.2006.11.009

633 Le Hir, P., Cann, P., Waeles, B., Jestin, H., Bassoulet, P., 2008. Erodibility of natural sediments: experiments on sand/mud
634 mixtures from laboratory and field erosion tests. Proceedings in Marine Science 9, 137-153. https://doi.org/10.1016/S1568-
635 2692(08)80013-7

636 Legout, C., Poulenard, J., Nemery, J., Navratil, O., Grangeon, T., Evrard, O., Esteves, M., 2013. Quantifying suspended sediment
637 sources during runoff events in headwater catchments using spectrocolorimetry. Journal of Soils and Sediments 13, 1478–1492.
638 https://doi.org/10.1007/s11368-013-0728-9

639 Legout, C., Droppo, I.G., Coutaz, J., Bel, C., Jodeau, M., 2018. Assessment of erosion and settling properties of fine sediments
640 stored in cobble bed rivers: the Arc and Isère alpine rivers before and after reservoir flushing: Erosion and settling dynamics of
641 fine sediments in cobble bed rivers. Earth Surf. Process. Landforms 43, 1295–1309. https://doi.org/10.1002/esp.4314

642 Legout, C., Freche, G., Biron, R., Esteves, M., Navratil, O., Nord, G., Uber, M., Grangeon, T., Hachgenei, N., Boudevillain, B.,
643 Voiron, C., Spadini, L., 2021. A critical zone observatory dedicated to suspended sediment transport: The meso-scale Galabre
644 catchment (southern French Alps). Hydrological Processes 35. https://doi.org/10.1002/hyp.14084

645 Lick W, McNeil J. 2001. Effects of sediment bulk properties on erosion rates. Science of the Total Environment 266(1–3), 41–48.
646 https://doi.org/10.1016/S0048-9697(00)00747-6

647 Liu, X.-L., Zheng, J.-W., Zhang, H., Zhang, S.-T., Liu, B.-H., Shan, H.-X., Jia, Y.-G., 2018. Sediment critical shear stress and
648 geotechnical properties along the modern Yellow River Delta, China. Marine Georesources & Geotechnology 36, 875–882.
649 https://doi.org/10.1080/1064119X.2017.1393477

650 Meng, X., Jia, Y., Shan, H., Yang, Z., Zheng, J., 2012. An experimental study on erodibility of intertidal sediments in the Yellow
651 River delta. International Journal of Sediment Research 27, 240–249. https://doi.org/10.1016/S1001-6279(12)60032-8

652 Misset, Clément, Recking, A., Navratil, O., Legout, C., Poirel, A., Cazilhac, M., Briguet, V., Esteves, M., 2019. Quantifying bed-
653 related suspended load in gravel bed rivers through an analysis of the bedload-suspended load relationship. Earth Surface
654 Processes and Landforms. https://doi.org/doi: 10.1002/esp.4606

655 Misset, C., Recking, A., Legout, C., Viana-Bandeira, B., Poirel, A., 2021. Assessment of fine sediment river bed stocks in seven
656 Alpine catchments. CATENA 196, 104916. https://doi.org/10.1016/j.catena.2020.104916

657 Navratil, O., Legout, C., Gateuille, D., Esteves, M., Liebault, F., 2010. Assessment of intermediate fine sediment storage in a
658 braided river reach (southern French Prealps). Hydrological Processes 1318–1332. https://doi.org/10.1002/hyp.7594

659 Navratil, O., Evrard, O., Esteves, M., Legout, C., Ayrault, S., Némery, J., Mate-Marin, A., Ahmadi, M., Lefèvre, I., Poirel, A., Bonté,
660 P., 2012. Temporal variability of suspended sediment sources in an alpine catchment combining river/rainfall monitoring and
661 sediment fingerprinting: TEMPORAL VARIABILITY OF SUSPENDED SEDIMENT SOURCES IN MOUNTAINS. Earth Surface Processes
662 and Landforms 37, 828–846. https://doi.org/10.1002/esp.3201

663 Némery,J., Mano, V., Coynel, A., Etcheber, H., Moatar,F., Meybeck, M., Belleudy, P., & Poirel A., 2013. Carbon and suspended
664 sediment transport in an impounded alpine river (Isère, France). Hydrological Processes 27, 2498–2508.
665 https://doi.org/10.1002/hyp.9387

666 Noack, M., Gerbersdorf, S., Hillebrand, G., Wieprecht, S., 2015. Combining Field and Laboratory Measurements to Determine the
667 Erosion Risk of Cohesive Sediments Best. Water 7, 5061–5077. https://doi.org/10.3390/w7095061

668 Partheniades, E., 1965. Erosion and deposition of cohesive soils. Journal of the Hydraulics Division, 91(1), 105-139.
669 https://doi.org/10.1061/JYCEAJ.0001165

670 Rainato, R., Mao, L., & Picco, L., 2020. The effects of low-magnitude flow conditions on bedload mobility in a steep mountain
671 stream. Geomorphology, 367, 107345. https://doi.org/10.1016/j.geomorph.2020.107345

672 Serlet, A. J., Gurnell, A. M., Zolezzi, G., Wharton, G., Belleudy, P., & Jourdain, C. 2018. Biomorphodynamics of alternate bars in a
673 channelized, regulated river: An integrated historical and modelling analysis. Earth Surface Processes and Landforms, 43(9),
674 1739-1756. https://doi.org/10.1002/esp.4349

675 Shields, A. 1936. Application of similarity principles and turbulence research to bed-load movement.

676 Singh, H.V., Thompson, A.M., 2016. Effect of antecedent soil moisture content on soil critical shear stress in agricultural
677 watersheds. Geoderma 262, 165–173. https://doi.org/10.1016/j.geoderma.2015.08.011

678 Syvitski, J.P.M., 2005. Impact of Humans on the Flux of Terrestrial Sediment to the Global Coastal Ocean. Science 308, 376–380.
679 https://doi.org/10.1126/science.1109454

680 Thollet, F., Rousseau, C., Camenen, B., Boubkraoui, S., Branger, F., Lauters, F., Némery, J., 2021. Long term high frequency
681 sediment observatory in an alpine catchment: The ARC-ISÈRE rivers, France. Hydrological Processes 35.
682 https://doi.org/10.1002/hyp.14044

683 Tolhurst, T.J., Black, K.S., Shayler, S.A., Mather, S., Black, I., Baker, K., Paterson, D.M., 1999. Measuring the in situ Erosion Shear
684 Stress of Intertidal Sediments with the Cohesive Strength Meter (CSM). Estuarine, Coastal and Shelf Science 49, 281–294.
685 https://doi.org/10.1006/ecss.1999.0512

686 Tolhurst, T.J., Black, K.S., Paterson, D.M., Mitchener, H.J., Termaat, G.R., Shayler, S.A., 2000. A comparison and measurement
687 standardisation of four in situ devices for determining the erosion shear stress of intertidal sediments. Continental Shelf
688 Research 20, 1397–1418. https://doi.org/10.1016/S0278-4343(00)00029-7

689 Tolhurst, T.J., Defew, E.C., de Brouwer, J.F.C., Wolfstein, K., Stal, L.J., Paterson, D.M., 2006. Small-scale temporal and spatial
690 variability in the erosion threshold and properties of cohesive intertidal sediments. Continental Shelf Research 26, 351–362.
691 https://doi.org/10.1016/j.csr.2005.11.007

692 Tolhurst, T.J., Black, K.S., Paterson, D.M., 2009. Muddy Sediment Erosion: Insights from Field Studies. Journal of Hydraulic
693 Engineering 135, 73–87. https://doi.org/10.1061/(ASCE)0733-9429(2009)135:2(73)

694 Truman, C. C., & Bradford, J. M., 1990. Effect of antecedent soil moisture on splash detachment under simulated rainfall. Soil
695 Science, 150(5), 787-798.

696 Uber, M., Nord, G., Legout, C., & Cea, L., 2021. How do modeling choices and erosion zone locations impact the representation
697 of connectivity and the dynamics of suspended sediments in a multi-source soil erosion model?. Earth Surface Dynamics, 9(1),
698 123-144. https://doi.org/10.5194/esurf-9-123-2021

699 van Rijn, L.C., 2020. Erodibility of Mud–Sand Bed Mixtures. J. Hydraul. Eng. 146, 04019050.
700 https://doi.org/10.1061/(ASCE)HY.1943-7900.0001677

701 Watts, C.W., Tolhurst, T.J., Black, K.S., Whitmore, A.P., 2003. In situ measurements of erosion shear stress and geotechnical
702 shear strength of the intertidal sediments of the experimental managed realignment scheme at Tollesbury, Essex, UK. Estuarine,
703 Coastal and Shelf Science 58, 611–620. https://doi.org/10.1016/S0272-7714(03)00139-2

Widdows, J., Friend, P.L., Bale, A.J., Brinsley, M.D., Pope, N.D., Thompson, C.E.L., 2007. Inter-comparison between five devices for determining erodability of intertidal sediments. Continental Shelf Research 27, 1174–1189. https://doi.org/10.1016/j.csr.2005.10.006

Wilkes, M.A., Gittins, J.R., Mathers, K.L., Mason, R., Casas-Mulet, R., Vanzo, D., Mckenzie, M., Murray-Bligh, J., England, J., Gurnell, A., Jones, J.I., 2018. Physical and biological controls on fine sediment transport and storage in rivers. Wiley Interdisciplinary Reviews: Water, 6(2), e1331. https://doi.org/10.1002/wat2.1331

Wood, P.J., Armitage, P.D., 1999. Sediment deposition in a small lowland stream-management implications. Regulated Rivers: Research & Management: An International Journal Devoted to River Research and Management, 15(1-3), 199-210. https://doi.org/10.1002/(SICI)1099-1646(199901/06)15:1/3%3C199::AID-RRR531%3E3.0.CO;2-0

Zabaleta, A., Martínez, M., Uriarte, J. A., & Antigüedad, I., 2007. Factors controlling suspended sediment yield during runoff events in small headwater catchments of the Basque Country. Catena, 71(1), 179-190. https://doi.org/10.1016/j.catena.2006.06.007

Spatial variability of the erodibility of fine sediments deposited in two alpine gravel-bed rivers: The Isère and Galabre

Aim of the study

(i) Assess spatial variability of the erodibility of fine sediment deposits in mountainous rivers

(ii) Investigate the main controlling factors of erodibility

Study sites and methodology

- Two gravel bed rivers in the French Alps: the Isère and Galabre rivers
- Erodibility (CSM device), grain size and moisture (probe) measurements on different deposit areas on both study sites

Main results

- Very high variability of critical erosion threshold : threshold ranging from 0 to 9 Pa.
- Structuration on the transect scale : medium altitude deposits are the most resistant.
- Correlation with moisture : Medium moisture deposits are the most resistant.

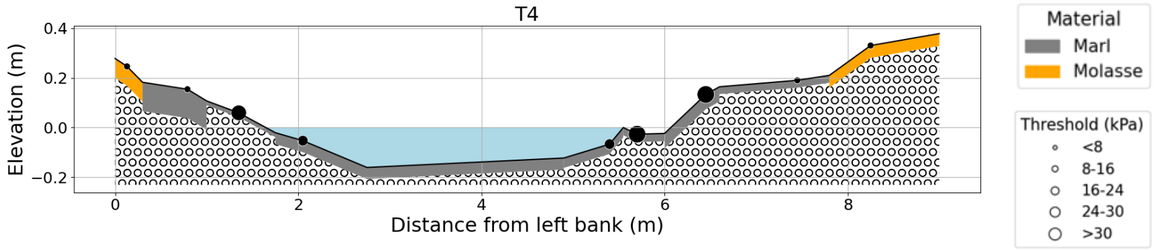

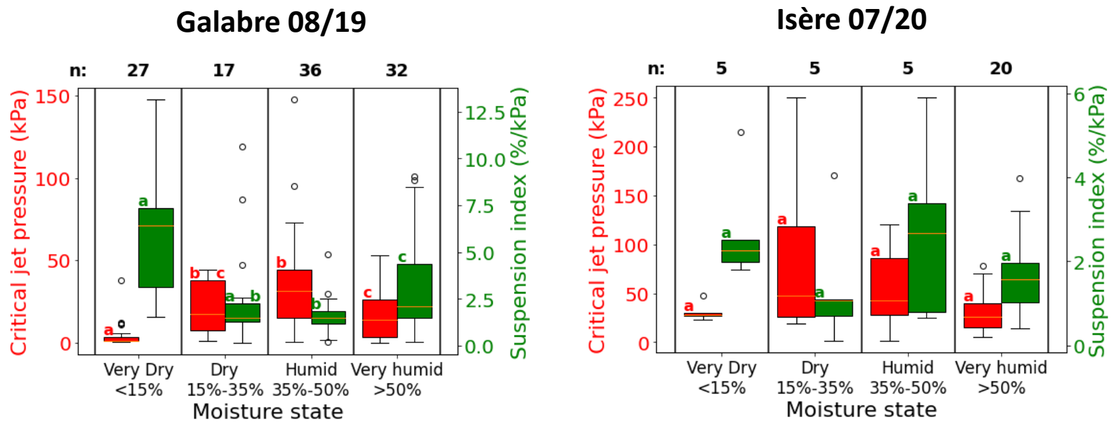

CSM device :

- In situ measurements of the erodibility of fine sediment deposits with the Cohesive Strength-Meter (CSM) device.

- Extraction of the critical jet pressure and suspension index from the CSM signal

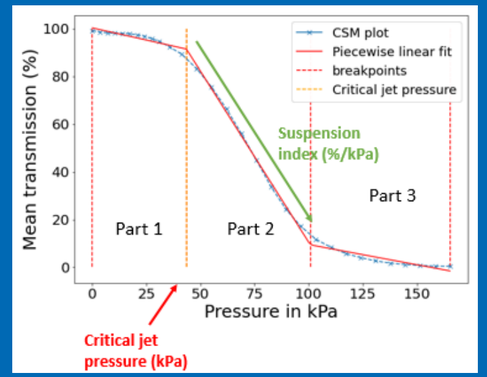

Hanna Haddad, hanna.haddad1995@gmail.com
Magali Jodeau, Cédric Legoût, Germain Antoine & Ian G. Droppo.